1 **Evaluation of [^{18}F]pitavastatin as a positron emission tomography probe for *in vivo***

2 **organic transporter polypeptide function**

3

4 Yusuke Yagi[a,b#], Hiroyuki Kimura[a,b#*], Haruka Okuda[a], Masahiro Ono[a], Yuji Nakamoto[c],

5 Kaori Togashi[c], Hideo Saji[a*]

6

7 [a]Department of Patho-Functional Bioanalysis, Graduate School of Pharmaceutical Sciences,

8 Kyoto University, 46-29 Yoshida Shimoadachi-cho, Sakyo-ku, Kyoto 606-8501, Japan

9 [b]Department of Analytical and Bioinorganic Chemistry, Kyoto Pharmaceutical University, 5

10 Nakauchi-cho, Misasagi, Yamashina-ku, Kyoto 607-8414, Japan

11 [c]Department of Diagnostic Imaging and Nuclear Medicine, Kyoto University Graduate

12 School of Medicine, 54 Shogoin Kawahara-cho, Sakyo-ku, Kyoto 606-8507, Japan

13

14 [#]These authors contributed equally to this work.

15

16 *Corresponding authors:

17 Hiroyuki Kimura, PhD and Hideo Saji, PhD

18 Department of Patho-Functional Bioanalysis, Graduate School of Pharmaceutical Sciences,

19 Kyoto University; 46-29 Yoshida Shimoadachi-cho, Sakyo-ku, Kyoto 606-8501, Japan

1 Tel: +81-75-753-4556, Fax: +81-75-753-4568

2 E-mail: hkimura@mb.kyoto-phu.ac.jp, hsaji@pharm.kyoto-u.ac.jp

3

1 **Abstract**

2 **Introduction:** To understand the pathways involved in drug clearance from the body,

3 quantitative evaluations of the hepatobiliary transport of drugs are important. The organic

4 anion transporting polypeptide (OATP) family transporter, particularly OATP1B1 and 1B3,

5 are considered to play an important role in hepatic uptake of organic anion compounds.

6 Pitavastatin is a substrate of OATP, and it includes a fluorine group. Therefore, it represents

7 an acceptable positron-emission tomography (PET) probe using F-18 to image in vivo hepatic

8 transporter functions.

9 **Method:** [^{18}F]Pitavastatin was synthesized using the method we previously reported. To

10 evaluate the potential of [^{18}F]pitavastatin in PET imaging of in vivo OATP functions, we

11 investigated the hepatic uptake with/without rifampicin as an OATP inhibitor after

12 administration in normal SD rats. [^{18}F]Pitavastatin metabolite was evaluated using

13 reverse-phase thin-layer chromatography (TLC) autoradiography. We subsequently analyzed

14 the PET image results and demonstrated that [^{18}F]pitavastatin selectively accumulated in the

15 liver post-administration.

16 **Result and discussion:** In metabolite analysis using reverse-phase TLC, we found that the

17 radioactivity detected in the plasma, liver (>90% intact), and bile mostly originated from the

18 parent pitavastatin of the PET study (~40 min). [^{18}F]pitavastatin's hepatic uptake decreased

19 (approximately 76%) with rifampicin co-administration in PET analysis. Because

1 [^{18}F]pitavastatin has lower clearance in rats than other previously reported OATP1B PET

2 probes, it holds the potential of an imaging probe that has a higher sensitivity in monitoring

3 hepatic OATP1B function's changes.

4 **Conclusion:** Compared with the previously reported OATP imaging probes, [^{18}F]pitavastatin

5 is more suitable for the sensitive detection of functional changes in OATP transporters. We

6 believe that [^{18}F]pitavastatin enables quantitative analysis of the hepatobiliary transport

7 system for organic anion compounds.

8

9 **Keywords**

10 Organic anion transporting polypeptide; Positron-emission tomography; Fluorine-18;

11 Pitavastatin; Integration plot method

12

13 **Abbreviations**

14 *MRP2* multidrug resistance-associated protein 2, *OATP* organic anion transporting

15 polypeptide, *%ID* percentage of injected dose, *PET* positron-emission tomography, *ROI*

16 region of interest

17

1   Introduction

2   The assessment of hepatobiliary drug transport represents an important factor in

3   understanding the pathways involved in drug clearance from the body. In humans, numerous

4   uptake and efflux transporters are coordinately involved in the hepatobiliary transport of

5   drugs [1,2]. The organic anion transporting polypeptide (OATP) family transports substrates

6   in a Na+ ion-independent manner [3]. In particular, the OATPs 1B1 and 1B3 play an

7   important role in the hepatic uptake of organic anion compounds. These transporters are

8   selectively expressed in the human liver. Of note, they recognize substrates that have anions

9   of extremely diverse structures. Among the substrates, several drugs used in the clinic can be

10   identified (e.g., 3-hydroxy-3-methylglutaryl-coenzyme A (HMG-CoA) reductase inhibitors

11   (statins), angiotensin-converting enzyme inhibitors, angiotensin II receptor antagonists

12   (sartans), and various anticancer drugs) [4]. Altered functions of these transporters, caused by

13   drug–drug interactions and genetic polymorphisms of specific transporter isoforms, result in

14   changes not only of blood–drug concentrations but also of intrahepatic drug concentrations.

15   Based on the extended clearance concept, At present, human liver samples (i.e., frozen

16   hepatocytes and liver tissue blocks) are available, and prediction of liver uptake in humans is

17   possible. However, there is the need for the development of a more accurate quantification

18   method.

1   Nuclear medicine imaging technology is attracting attention as a functional diagnostic

2   method that enables noninvasive and specific molecular imaging with high sensitivity in

3   living systems. Among others, positron-emission tomography (PET) is superior to

4   single-photon emission computed tomography in terms of sensitivity and quantitative

5   analysis. In recent years, several PET probes (e.g., [11C]15R-TIC [5, 6],

6   [11C]dehydropravastatin [7, 8], [11C]telmisartan [9], [11C]rosuvastatin [10], and [18F]LCATD

7   [11]) have been developed to directly characterize in vivo the hepatobiliary transport systems

8   for organic anions (Figure 1) [6]. An important feature of PET probes for the quantification

9   of transport functions is that the probes themselves must not undergo extensive metabolism.

10   Otherwise, the pharmacokinetic parameters determined represent a complex of intrinsic

11   parameters for metabolism and membrane transport.

12   In addition, almost developed PET probes used to examine hepatobiliary transport were

13   previously labeled with 11C. While handling these compounds, time constraints were

14   considered. The higher achievable activity for production and the longer half-lives of

15   18F-labeled probes are clear advantages over 11C-probes for both pre-clinical and clinical PET

16   imaging. As a consequence, there still exists a need to develop 18F-labeled compounds with

17   longer half-lives. However, till date, 18F-tracer has only been developed as 18F-labeled bile

18   acid derivative [18F]LCATD. In the present study, pitavastatin, an antihyperlipidemic agent,

19   was selected as the maternal compound for the PET imaging probe. Pitavastatin clears

1   predominantly from the liver, where OATP1B1 and OATP1B3 play pivotal roles in its uptake

2   [12]. As a consequence, pitavastatin is expected to have a unique pharmacokinetic character.

3   Pitavastatin has a fluorine group in its structure. Therefore, by using ^{18}F, a PET nuclide, a

4   PET imaging probe can be made while maintaining the physical and chemical properties. In

5   an earlier study, we developed a synthetic method of [^{18}F]pitavastatin using the Suzuki

6   coupling reaction with 4-[^{18}F]fluoroiodobenzene ([^{18}F]FIB) [13] (Figure 1). In the present

7   study, we aimed at characterizing the hepatobiliary transport of [^{18}F]pitavastatin in rats by

8   PET imaging with co-administration of rifampicin, a typical OATP1B inhibitor.

9

10

1 **Materials and Methods**

2 *Materials*

3 All reagents and solvents used in the present study were commercially available. Specifically,

4 we purchased them from Wako Pure Chemical Industries (Tokyo, Japan), Nacalai Tesque

5 (Kyoto, Japan), Merck (Darmstadt, Germany), and Sigma Aldrich (St. Louis, MO, USA).

6 Reagents and solvents were used as received, without further purification. The identity and

7 concentration of [18F]pitavastatin were assessed by high-performance liquid chromatography.

8 To this end, we used a Shimadzu system (a LC-20AT pump with an SPD-20A UV detector,

9 σ=220, 254nm; Shimadzu, Kyoto, Japan) with a Cosmosil 5C18-AR-II column (4.6 × 150

10 mm and 10 × 250 mm; Nacalai Tesque) and a radioisotope detector.

11

12 *Synthesis of [18F]pitavastatin*

13 [18F]Pitavastatin was synthesized as previously reported [13].

14 **Radiochemistry**

15 [18F]Fluoride was produced using a cyclotron (CYPRIS HM-18, Sumitomo Heavy Industries,

16 Tokyo, Japan) via an ^{18}O (p,n) ^{18}F reaction and passed through a Sep-Pak Light QMA

17 cartridge (Waters Corporation, Milford, MA, USA) as an aqueous solution in ^{18}O-enriched

18 water. The cartridge was then dried using N_2, and ^{18}F activity was eluted using 1.0 mL of a

19 Kryptofix2.2.2 (Merck)/K_2CO_3 solution [9.5 mg of Kryptofix2.2.2 and 1.7 mg of K_2CO_3 in

20 MeCN/water (96/4)]. The solvent was removed by azeotropic dehydration with MeCN (1.0

21 mL) at 120°C under a stream of argon gas for 10 min.

22 **Synthesis of 4-[18F]Fluoroiodobenzene**

1   A solution of 4-iodophenyldiphenylsulfonium triflate (2.00 mg) in MeCN (150 μL) was

2   added to a reaction vessel containing the ^{18}F activity (1.10–1.50 GBq), and the reaction

3   mixture was heated for 1 min under microwave irradiation (50.0 W). The resulting mixture

4   was cooled for 1 min and then passed through a Sep-Pak Light C18 column (Waters) and

5   washed with water (10 mL). A stream of N$_2$ gas was passed over the column for 10 s, and

6   4-[^{18}F]fluoroiodobenzene was eluted using MeCN (500 μL). The eluent containing

7   4-[^{18}F]fluoroiodobenzene was purified using HPLC [radiochemical yield 56.2% ± 3.1%

8   decay corrected, data are the mean ± SD (n = 3)].

9   **Synthesis of [^{18}F]pitavastatin using the Suzuki-coupling**

10 A solution of [^{18}F]fluoroiodobenzene in MeCN (185–222 MBq, 100–150 μL) was added to a

11 solution of boronic ester precursor (2.0 mg), tris(dibenzylideneacetone)dipalladium(0) (1.0

12 mg) and cesiumcarbonate (4.0 mg) in MeCN (100 μL); the resulting mixture was heated to

13 100°C under microwave irradiation (50.0 W) for 1 min. The mixture was then passed through

14 the COSMONICE(R) Filter (S) (0.45 μm, 4 mm) and purified using preparative HPLC

15 [Cosmosil 5C18-ARII 10 × 250 mm column, MeOH/20 mM phosphate buffer (pH 2.5) =

16 70/30, flow rate 5.0 mL/min] to obtain a pure solution of [^{18}F]pitavastatin [Rt = 8.5 min,

17 radiochemical yield: 12.1% ± 3.0% decay corrected from [^{18}F]fluoride ions (mean ± SD, n =

18 3), radiochemical purity: >99%, molar activity: >10.0 GBq/μmol].

19

1   *Animals*

2   Male Sprague Dawley (SD) rats weighing 222–333 g (8–10 weeks old) were purchased from

3   Japan SLC, Inc. (Shizuoka, Japan). All animals were kept in a temperature- and

4   light-controlled environment with standard food. Tap water was provided ad libitum. All

5   animal procedures were approved by the Kyoto University Animal Care Committee.

6

7   **PET Scans**

8   All PET and computed tomography (CT) scans were performed using a FX-3300 (Gamma

9   Medica, Salem, NH, USA), specifically designed for laboratory animals. Specifically, this

10   PET scanner has a spatial resolution of <1 mm in full width at half-maximal at the center of

11   the view at 100 mm in diameter and an axial extent of 110 mm in length. Control SD rats

12   were used for PET experiments with [^{18}F]pitavastatin alone. Rats were anesthetized and

13   maintained under anesthesia with 1.5% isoflurane. Additionally, the femoral artery was

14   cannulated with polyethylene tubing for blood collection. At the start of the emission scan,

15   [^{18}F]pitavastatin was administered as a single bolus (<85.1 nmol) via the tail vein [dosage:

16   7.06 ± 1.49 MBq; data are presented as mean ± SD (n = 3)]. All PET acquisitions were

17   performed in dynamic scan mode for 60 min. Conversely, we intravenously infused

18   rifampicin, a typical inhibitor of OATP1Bs, to estimate the transport function of OATP1Bs in

19   the liver as an OATP inhibition model [7]. Rifampicin infusion occurred at a rate of 1.5

1　μmol/min/kg for at least 90 min prior to the administration of [^{18}F]pitavastatin. Additionally,

2　a constant infusion rate was maintained until the PET scan was concluded (in total, 50–75

3　μmol of rifampicin was used for blocking scan). Blood sampling time points were as follows:

4　10, 20, 30, 40, and 50 s and 1, 2, 5, 10, 20, and 30 min after bolus administration of

5　[^{18}F]pitavastatin. Additionally, the total blood volume sampled from each rat was maximum

6　160 μL, which did not exceed 1% of the total circulating blood volume (1.6 mL) as

7　approximately 10 μL of blood was sampled at each time point. Of note, such blood sampling

8　causes very less damage in rats. Blood radioactivity levels were measured using a μFmPC

9　system (Shimadzu). Radioactivity in each measured sample was corrected for decay.

10　Following the PET scan, CT scans were performed. To this end, the following conditions

11　were used: tube voltage, 60 kV; tube current, 310 μA. Anesthesia was maintained at 1.5%

12　isoflurane pre-euthanasia, using an injection of sodium pentobarbital.

13

14　***Analysis of PET Imaging***

15　PET images were reconstructed by Fourier rebinning and standard 3D ordered-subset

16　expectation maximization. Regions of interest (ROIs) representing the liver were delineated

17　using the Pmod program (v. 3.3; PMOD Technologies, Zurich, Switzerland). All the ROIs

18　were combined and transformed to volumetric ones. The time-radioactivity curve for the liver

1   was performed by normalizing decay-corrected time-radioactivity measurements to

2   [^{18}F]pitavastatin's injected dose (% dose).

3

4   ***Biodistribution of Radioactivity After [^{18}F]pitavastatin Administration***

5   Rats were injected in the tail vein with a saline solution of [^{18}F]pitavastatin. Animals were

6   sacrificed at specific time points [i.e., 2, 5, 10, 15, 30, and 60 min postinjection; data are

7   presented as mean ± SD (n = 5)]. We quickly removed samples of the blood, heart, lung, liver,

8   spleen, pancreas, stomach, intestine, kidney, bone, and whole brain. The tissues' radioactivity

9   was measured with a 1480 WIZARD 3 automatic gamma counter (PerkinElmer Co., Ltd.).

10 Finally, results were expressed as the percentage of the injected dose (%ID). All radioactivity

11 measurements were corrected for decay.

12

13 ***Analysis of Metabolites in the Blood, Bile, and Liver Using Thin-Layer Chromatography***

14 ***(TLC)***

15 Metabolite analysis was executed as previously described [6]. We first performed cannulation

16 of the femoral artery and the bile duct in the SD rat. Then, [^{18}F]pitavastatin was injected via

17 the tail vein at a dosage of 40MBq. Arterial blood samples were collected at 1, 2, 5, 10, 20,

18 and 40 min postinjection. Additionally, bile samples were collected at 0–5, 5–10, 10–25, and

19 25–40 min postinjection. In order to perform liver tissue sampling, blood flow was

1 terminated by transection of the abdominal aorta and vein at 10 and 40 min postinjection. The

2 liver was then quickly removed and homogenized. Additionally, precipitation with

3 acetonitrile was used to deproteinize blood, bile, and liver samples. After centrifugation

4 (12000 rpm, 2 min, 0°C), the supernatants were applied to RP-18 TLC plates (Merck KGaA,

5 Darmstadt, Germany).

6 Plates were developed at room temperature using acetonitrile/water/acetic acid (50:50:0.75)

7 as a mobile phase. After migration, plates were dried and exposed to BAS SR2040 imaging

8 plates (Fuji Film, Tokyo, Japan) for 90–360 min. Radioactivity's distribution on the imaging

9 plates was determined by digital PSL autoradiography using a Fuji BAS-5000 analyzer.

10 Subsequently, data was analyzed using the MultiGauge image analysis program (Fuji Film).

11 Rf value was determined pitavastatin and a lactone form of pitavastatin which was

12 synthesized [13].

13

14 ***Kinetic Analyses of PET Data to Determine the Clearance of Radioactivity***

15 Radioactivity's initial uptake clearance in the liver ($CL_{uptake,liver}$) was calculated by

16 integration plot analyzes [14]. To this end, the initial linear portion of the curves after

17 [^{18}F]pitavastatin administration (0.5–5 min) was used. The $CL_{uptake,liver}$ of [^{18}F]pitavastatin

18 was estimated based on the following equation:

19
$$\frac{X_{t,liver}}{C_{t,blood}} = CL_{uptake,liver} \times \frac{AUC_{0-t,blood}}{C_{t,blood}} + V_{E,liver}, \tag{1}$$

1   where $X_{t,liver}$, $C_{t,blood}$, and $AUC_{0-t,blood}$ represent the amount of radioactivity in the liver at time

2   t, the blood concentration of radioactivity at time t, and the area under the blood

3   concentration–time curve from time 0 to t, respectively. $V_{E,liver}$ represents the initial

4   distribution volume in the liver at time 0. This was calculated from the y intercept of the

5   integration plot. To estimate $AUC_{0-t,blood}$, radioactivity's blood concentration–time curve was

6   fitted to the following two-exponential equation:

7    $C_{B,t} = Ae^{-\alpha t} + Be^{-\beta t}$

8   to optimize parameters (α, β, A, B). Then, $AUC_{0-t,blood}$ was calculated by means of the

9   following equation:

10
$$AUC_{0-t,blood} = \frac{A}{\alpha} \cdot (1 - e^{-\alpha t}) + \frac{B}{\beta} \cdot \left(1 - e^{-\beta t}\right) \qquad (2)$$

11    $CL_{uptake,liver}$ was obtained from the initial slope of the plot of $X_{t,liver}/C_{t,blood}$ versus

12    $AUC_{0-t,blood}/C_{t,blood}$.

13

14   ***Statistical Analysis***

15   Student's two-tailed t-test was used to identify significant differences in the kinetic

16   parameters between control and rifampicin-treated rats. We considered as statistically

17   significant p-values <0.05.

18

19

1 **Results and Discussion**

2 ***Radiometabolite Analysis of [^{18}F]pitavastatin in the Blood, Liver, and Bile by TLC***

3 ***Autoradiography***

4 Figure 2 shows TLC radiograms in which the extract from plasma, liver, and bile after

5 [^{18}F]pitavastatin administration was developed by reverse-phase TLC, respectively. In the

6 present study, we showed that virtually no metabolites were detectable in the blood. When

7 evaluating the liver extracts, we found that one metabolite (M1) was barely detectable

8 following the administration of [^{18}F]pitavastatin. However, almost all radioactivity was

9 derived from intact [^{18}F]pitavastatin (94.6% at 40 min, Supplemental table 1). As for bile

10 extracts, we identified a lactone form of pitavastatin [13] and two metabolites (M1 and M2).

11 However, 81.9% of the radioactivity was derived from intact [^{18}F]pitavastatin, 40 min after

12 [^{18}F]pitavastatin administration (Supplemental table 1).

13 Results of this study showed that [^{18}F]pitavastatin's metabolite analysis was in line with

14 previous reports on [^{14}C]pitavastatin [15, 16]. In the case of [^{14}C]pitavastatin, a previous

15 study showed that 84, 95, and 85% of the total radioactivity was derived from pitavastatin in

16 the plasma, liver, and bile 60 min post-intravenous administration of [^{14}C]pitavastatin,

17 respectively [15, 16]. Of note, these results indicated that most of the radioactivity was

18 derived from [^{18}F]pitavastatin. Therefore, we believe that the kinetic parameters estimated

19 from the present PET study correctly reflect pitavastatin's hepatobiliary transport.

1 *Biodistribution of Radioactivity and Effect of Rifampicin Co-administration in the*

2 *Abdominal Region Post-intravenous Administration of [^{18}F]pitavastatin*

3 Figure 3 shows the PET image of normal SD rat with/without rifampicin as an OATP

4 inhibitor after [^{18}F]pitavastatin administration. Additionally, it presents the analysis results

5 from PET images using the Pmod program. In the control rats' liver, a maximum of

6 48.1±1.5% of the injected dose was distributed 8 min post-administration of [^{18}F]pitavastatin.

7 Additionally, we found a decrease of radioactivity until the PET scan's end (39.3±1.27%ID at

8 30 min). Results of the biodistribution study in normal SD rats over time showed that

9 radioactivity was predominantly present in the liver in the early phase (71.5±3.4%ID at 10

10 min, Table 1). It then gradually decreased by the end of the examination (54.1±5.1%ID at 30

11 min). Additionally, we observed that radioactivity's reduction rates in the liver were similar

12 among PET scan and biodistribution study. Furthermore, data error was small. These results

13 suggest that the PET analysis of [^{18}F]pitavastatin was appropriately consistent compared with

14 the biodistribution study. On the contrary, radioactivity was also detected post-administration

15 of [^{18}F]pitavastatin in the kidney at early time points and in the intestine at a later time point

16 (30 min). However, similarly to a separate conventional biodistribution study, in the PET

17 scan, no clear distribution of radioactivity to other tested organs was observed (Table 1).

18 These results are consistent with a previous study of [^{14}C]pitavastatin. Specifically, an earlier

19 whole-body autoradiography of rats that received an intravenous administration of

1   [14C]pitavastatin indicated that radioactivity mainly accumulated in the liver and kidney at

2   2.5 min, while high levels of radioactivity were found in the liver and intestine 60 min

3   post-administration [15, 16]. We think that OATP1A2 expressed in the kidney affected early

4   uptakepitavastatin as this drug has less contribution to OATP1A2 compared with that to

5   OATP1B1 [3, 17,]. In rifampicin-treated rats, as shown in Figure 3, we found that the

6   amount of radioactivity accumulated in the liver and intestine was noticeably less than in

7   control rats (no rifampicin). Furthermore, the liver's maximum radioactivity ($31.6 \pm 4.9\%$ at

8   8 min) decreased to 65% compared with control rats ($p < 0.05$; Student's two-tailed t-test).

9   Such results suggested that the hepatobiliary transport of [18F]pitavastatin was modified by

10   co-administration with rifampicin, an OATP inhibitor. On the contrary, radioactivity's blood

11   concentration became significantly higher even 2 min after [18F]pitavastatin administration vs.

12   control rats. Furthermore, radioactivity levels in the liver and intestine were found to be

13   significantly lower. In the present study, the protocol of rifampicin administration used

14   (constant infusion of 1.5 μmol/min/kg for >90 min) was the same as the one used in previous

15   PET studies with [11C]dehydropravastatin and [11C]telmisartan [7, 9]. Specifically, unbound

16   blood concentration of rifampicin was 11–13 μM at steady state in rats. This value is

17   sufficiently high to potently inhibit rat Oatp1a4 ($K_i = 1.46$ μM) and Oatp1b2 ($K_i = 0.79$ μM)

18   and to partly inhibit rat Oatp1a1 ($K_i = 18.2$ μM) [18, 19].

19

1   *Kinetic Analyses of PET Data to Determine Radioactivity's Clearance*

2   Radioactivity in blood samples was eliminated in a biphasic manner in both control and

3   rifampicin-treated rats (Fig. 3C). However, with co-administration of rifampicin,

4   radioactivity's elimination was delayed. Additionally, its blood AUC_{0-30}, normalized by

5   [^{18}F]pitavastatin's dose, was 3.4-fold larger in rifampicin-treated rats [111.4 ± 34.9 (% of

6   dose/mL*min)] than in control SD rats [33.1 ± 5.0 (% of dose/mL*min); $p < 0.05$; Student's

7   two-tailed t-test]. Similarly, these results indicate that blood concentration increased due to

8   liver uptake inhibition by rifampicin. Integration plots for hepatic uptake clearance

9   ($CL_{uptake,liver}$) are shown in Figure 4A, and their kinetic parameters are summarized in Figure

10 4B. Linearity of the plot was maintained for a short time period between 0.5–5 min for liver

11 uptake. In control rats, $CL_{uptake,liver}$ was 9.08 ± 1.33 mL/min/kg, while in rifampicin-treated

12 rats, $CL_{uptake,liver}$ significantly decreased to 26% of the control values (2.33 ± 0.11 mL/min/kg,

13 $p < 0.05$; Student's two-tailed t-test). Of note, the degree of decrease in $CL_{uptake,liver}$ of

14 [^{18}F]pitavastatin was noticeably smaller with respect to previous reported probes as

15 [^{11}C]telmisartan (65% of control) and [^{11}C]dehydropravastatin (69% of control) [7, 9]. These

16 differences can partially be explained by the fact that the $CL_{uptake,liver}$ values of

17 [^{11}C]telmisartan (63 ± 11 mL/min/kg) [7] and [^{11}C]dehydropravastatin (73.6 ± 4.8

18 mL/min/kg) [9] were almost equal to the hepatic blood flow rate (55 mL/min/kg). This result

19 implies that it was difficult to accurately calculate the intrinsic hepatic uptake clearance in

1   rats [20, 21]. Conversely, this value of [^{18}F]pitavastatin (9.08 $\pm$ 1.33 mL/min/kg) was

2   one-sixth of the hepatic blood flow rate. Therefore, we believe that [^{18}F]pitavastatin can be

3   used to estimate the intrinsic hepatic uptake clearance in rats in an *in vivo* PET study.

4   Furthermore, pitavastatin's in vitro uptake clearance in rat hepatocytes was reported to be

5   121–444 μL/min/mg protein [22, 23]. The latter corresponds to a $CL_{uptake,liver}$ of 10.4–26.1

6   mL/min/kg, assuming a well-stirred model with physiological scaling factors (1.2 $\times$

7   10^8cells/g liver, 41.2 g liver/kg; f_B of pitavastatin in rats, 0.021) [23, 24]. Thus, hepatic

8   clearance determined from the *in vitro* study of pitavastatin is similar to that determined from

9   the PET analysis of [^{18}F]pitavastatin. As a result, [^{18}F]pitavastatin has the potential of a

10   higher sensitivity in detecting the inhibitory effects of drugs on hepatic OATP1B transporters

11   vs. other reported OATP imaging probes.

12

13

1 **Conclusion**

2 In summary, in the present feasibility study, the kinetic analyzes of [^{18}F]pitavastatin's

3 hepatobiliary transport in rats were carried out using PET imaging. As expected,

4 intravenously infusion of rifampicin, a typical OATP inhibitor, reduced hepatic uptake. Such

5 findings confirmed that, in the rat's liver, [^{18}F]pitavastatin's membrane transport was

6 predominantly transporter mediated. [^{18}F]pitavastatin can quantitatively detect changes in the

7 hepatobiliary transport of an OATP inhibition model of rats. Compared with previously

8 reported OATP imaging probes, especially [^{11}C]dehydropravastatin and [^{11}C]telmisartan, we

9 can found that [^{18}F]pitavastatin is suitable for the sensitive detection of functional changes in

10 OATP transporters. We believe that this finding is due to drug–drug interactions and genetic

11 polymorphisms of specific transporter isoforms by [^{18}F]pitavastatin. Of note,

12 [^{18}F]pitavastatin's hepatic clearance was not limited by hepatic blood flow rate. Pitavastatin

13 has been used as an antihyperlipidemic drug for many years. We believe that the

14 pharmacokinetic properties identified here are also applicable to humans. Specifically, we

15 expect that [^{18}F]pitavastatin performs similarly in detecting functional changes in OATP1Bs

16 in human PET studies.

17
18

13

1 **References**

2 [1] K. Yoshida, K. Maeda, Y. Sugiyama, Hepatic and intestinal drug transporters: prediction

3 of pharmacokinetic effects caused by drug-drug interactions and genetic polymorphisms.

4 Annu. Rev. Pharmacol. Toxicol. 2013;53:581–612.

5 https://doi.org/10.1146/annurev-pharmtox-011112-140309.

6 [2] M.J. Zamek-Gliszczynski, M.E. Taub, P.P. Chothe, et al., Transporters in drug

7 development: 2018 ITC recommendations for transporters of emerging clinical importance.

8 Clin. Pharmacol. Ther. 2018;104:890–899. https://doi.org/10.1002/cpt.1112

9 [3] A. Obaidat, M. Roth, B. Hagenbuch, The expression and function of organic anion

10 transporting polypeptides in normal tissues and in cancer, Annu. Rev. Pharmacol. Toxicol.

11 2012;52:135–151. https://doi.org/10.1146/annurev-pharmtox-010510-100556.

12 [4] K. Maeda, H, Suzuki, Y, Sugiyama, Hepatic Transport in: Drug Bioavailability

13 Wiley-VCH Verlag GmbH; 2009, chapter 11, p 277–332.

14 https://doi.org/10.1002/9783527623860.ch11.

15 [5] T. Takashima, S. Kitamura, Y. Wada, et al., PET imaging-based evaluation of

16 hepatobiliary transport in humans with (15R)-^{11}C-TIC-Me. J. Nucl. Med. 2012;53:741–748.

17 https://doi.org/10.2967/jnumed.111.098681.

18 [6] T. Takashima, H. Nagata, T. Nakae, et al., Positron emission tomography studies using

19 (15R)-16-m-[11C]tolyl-17,18,19,20-tetranorisocarbacyclin methyl ester for the evaluation of

hepatobiliary transport. J. Pharmacol. Exp. Ther. 2010;335:314–323. https://doi.org/10.1124/jpet.110.170092.

[7] T. Shingaki, T. Takashima, R. Ijuin, et al., Evaluation of Oatp and Mrp2 activities in hepatobiliary excretion using newly developed positron emission tomography tracer [^{11}C]dehydropravastatin in rats. J. Pharmacol. Exp. Ther. 2013;347:193–202. https://doi.org/10.1124/jpet.113.206425.

[8] K. Kaneko, M. Tanaka, A. Ishii, et al., A clinical quantitative evaluation of hepatobiliary transport of [^{11}C]dehydropravastatin in humans using positron emission tomography. Drug. Metab. Dispos. 2018;46:719–728. https://doi.org/10.1124/dmd.118.080408.

[9] T. Takashima, Y. Hashizume, Y. Katayama, et al., The involvement of organic anion transporting polypeptide in the hepatic uptake of telmisartan in rats: PET studies with [^{11}C]telmisartan. Mol. Pharm. 2011;8:1789–1798. https://doi.org/10.1021/mp200160t.

[10] J. He, Y. Yu, B. Prasad, et al., PET imaging of Oatp-mediated hepatobiliary transport of [^{11}C]rosuvastatin in the rat. Mol. Pharm. 11 2014;11:2745–2754. https://doi.org/10.1021/mp500027c.

[11] A. Testa, S. Angelo, M. Mingarelli, et al., Design, synthesis, in vitro characterization and preliminary imaging studies on fluorinated bile acid derivatives as PET tracers to study hepatic transporters. Bioorg. Med. Chem. 2017;25:963–976. https://doi.org/10.1016/j.bmc.2016.12.008.

1 [12] M. Hirano, K. Maeda, Y. Shitara, et al., Contribution of OATP2 (OATP1B1) and

2 OATP8 (OATP1B3) to the hepatic uptake of pitavastatin in humans. J. Pharmacol. Exp. Ther.

3 2004;311:139–146. https://doi.org/10.1124/jpet.104.068056.

4 [13] Y. Yagi, H. Kimura, K. Arimitsu, et al., The synthesis of [^{18}F]pitavastatin as a tracer for

5 hOATP using the Suzuki coupling. Org. Biomol. Chem. 2015;13:1113–1121.

6 https://doi.org/10.1039/c4ob01953a.

7 [14] D. C. Kim, Y. Sugiyama, M. Hanano, Kinetic analysis of in vivo receptor-dependent

8 binding of human epidermal growth factor by rat tissues. J. Pharm. Sci. 1988;77 (3):200–207.

9 https://doi.org/10.1002/jps.2600770304

10 [15] H. Kimata, H. Fujino, T. Koide, et al., Studies on the metabolic fate of NK-104, a new

11 inhibitor of HMG-CoA reductase (1): absorption, distribution, metabolism and excretion in

12 Rats. Drug. Metab. Pharmacokinet. 1998;13:484–499. https://doi.org/10.2133/dmpk.13.484.

13 [16] H. Fujino, Y. Tsunenari, T. Koide, et al., Studies on the Metabolic Fate of NK-104, a

14 New Inhibitor of HMG-CoA Reductase. (2). Absorption, Distribution, Metabolism, Excretion

15 and Accumulation Following Repeated Oral Administration of ^{14}C-NK-104 in Rats. Drug.

16 Metab. Pharmacokin. 1998;13(5):499–507. https://doi.org/10.2133/dmpk.13.499

17 [17] Y. Shirasaka, K. Suzuki, M. Shichiri, et al., Intestinal absorption of HMG-CoA

18 reductase inhibitor pitavastatin mediated by organic anion transporting polypeptide and

P-glycoprotein/multidrug resistance 1. Drug Metab. Pharmacokinet. 2011;26 (2):171–179. https://doi.org/10.2133/dmpk.DMPK-10-RG-073

[18] Y. Shitara, D. Sugiyama, H. Kusuhara, et al., Comparative inhibitory effects of different compounds on rat oatpl (slc21a1)- and Oatp2 (Slc21a5)-mediated transport. Pharm. Res. 2002;19:147–153. http://dx.doi.org/10.1023/A:1014264614637.

[19] Y.Y. Lau, H. Okochi, Y. Huang, et al., Multiple transporters affect the disposition of atorvastatin and its two active hydroxy metabolites: application of in vitro and ex situ systems. J. Pharmacol. Exp. Ther. 2006;316:762–771. https://doi.org/10.1124/jpet.105.093088.

[20] M.S. Roberts, M. Rowland, Correlation between in‐vitro microsomal enzyme activity and whole organ hepatic elimination kinetics: analysis with a dispersion model. J. Pharm. Pharmacol. 1986;38(3):177–181. https://doi.org/10.1111/j.2042-7158.1986.tb04540.x.

[21] T. Iwatsubo, N. Hirota, T. Ooie, et al., Prediction of in vivo drug metabolism in the human liver from in vitro metabolism data. Pharmacol. Ther. 1997;73(2):147–171. https://doi.org/10.1016/S0163-7258(96)00184-2.

[22] S. Shimada, H. Fujino, T. Morikawa, et al., Uptake mechanism of pitavastatin, a new inhibitor of HMG-CoA reductase, in rat hepatocytes. Drug. Metab. Pharmacokinet. 2003;18:245–251. https://doi.org/10.2133/dmpk.18.245.

1 [23] T. Watanabe, H. Kusuhara, K. Maeda, et al., Investigation of the rate-determining

2 process in the hepatic elimination of HMG-CoA reductase inhibitors in rats and humans.

3 Drug. Metab. Dispos. 2010;38:215–222. https://doi.org/10.1124/dmd.109.030254.

4 [24] T. Watanabe, H. Kusuhara, K. Maeda. et al., Physiologically based pharmacokinetic

5 modeling to predict transporter-mediated clearance and distribution of pravastatin in humans.

6 J. Pharmacol. Exp. Ther. 2009;328(2):652–662. https://doi.org/10.1124/jpet.108.146647

7

8

9

10

1

2

3 **Table 1**. Time-dependent tissue distribution of radioactivity after intravenous administration

4 of [^{18}F]pitavastatin.

	%ID/organ ± SD (n = 5)					
	2 min	5 min	10 min	15 min	30 min	60 min
Blood[a]	11.63±1.31	4.57±0.59	2.80±0.21	1.97±0.15	1.26±0.16	1.35±0.75
Heart	0.19±0.01	0.12±0.01	0.11±0.01	0.11±0.01	0.12±0.02	0.12±0.04
Lung	0.30±0.02	0.18±0.04	0.11±0.02	0.09±0.02	0.03±0.01	0.06±0.03
Liver	69.56±1.66	70.11±2.74	71.54±3.40	68.05±6.38	54.11±5.13	32.61±3.69
Pancreas	0.22±0.08	0.06±0.03	0.06±0.02	0.05±0.04	0.03±0.02	0.04±0.02
Spleen	0.08±0.01	0.04±0.01	0.02±0.00	0.02±0.01	0.01±0.01	0.02±0.02
Stomach	0.18±0.03	0.29±0.21	0.10±0.10	0.34±0.31	0.28±0.33	0.12±0.04
Intestine	4.00±0.30	8.20±0.90	13.33±3.72	20.22±2.79	33.78±5.74	64.86±7.72
Kidney	7.46±0.37	2.13±0.34	1.25±0.27	0.97±0.25	0.68±0.10	0.55±0.19
Bone[b]	0.12±0.02	0.07±0.01	0.04±0.01	0.04±0.02	0.04±0.04	0.02±0.03

5 [a] Assuming that weight of blood in rats was 10% of total body weight. [b] data is presented

6 as %ID/g.

7

1   **Figure legends**

2   **Figure 1**. Chemical structure of the PET probe for OATP evaluation. (A) [^{11}C]15R-TIC-Me,

3   (B) [^{11}C]dehydropravastatin, (C) [^{11}C]telmisartan, (D) [^{11}C]rosuvastatin, (E) [^{18}F]pitavastatin

4   (present study)

5

6   **Figure 2.** Representative TLC autoradiograms on the radio metabolite analysis following

7   intravenous administration of [^{18}F]pitavastatin in normal rat.

8   Each line represents an authentic [^{18}F]pitavastatin sample [pitavastatin (aus.)] and blood, liver,

9   and bile extract samples collected at the designated time points following [^{18}F]pitavastatin's

10   intravenous administration. We have confirmed that pitavastatin lactone band's location is

11   identical to the Rf values of the pitavastatin lactone that we created (Rf=0.13–0.14)

12

13   **Figure 3.** PET images of rat abdominal regions taken post-intravenous administration of

14   [^{18}F]pitavastatin (anesthesia: 1.5% isoflurane; dosage: 7.06 ± 1.49 MBq; n = 3). Colonal

15   maximum intensity projecting PET images of radioactivity in the abdominal region were

16   captured at 2, 5, 10, 20, and 30 min in control rats (A), rifampicin-treated rats at an infusion

17   rate of 1.5μmol/min/kg (B).

18   Radioactivity's time profiles in blood from the μFmPC system (C) and liver were determined

19   by PET imaging analysis 30 min post-intravenous administration of [^{18}F]pitavastatin. (D)

20   Each symbol represents the control and rifampicin-treated rats (1.5 mmol/min/kg for at least a

1 90 min PET scan). The data represent the mean ±SD. (n=3; Students t-test, * $p<0.05$, †<0.01,

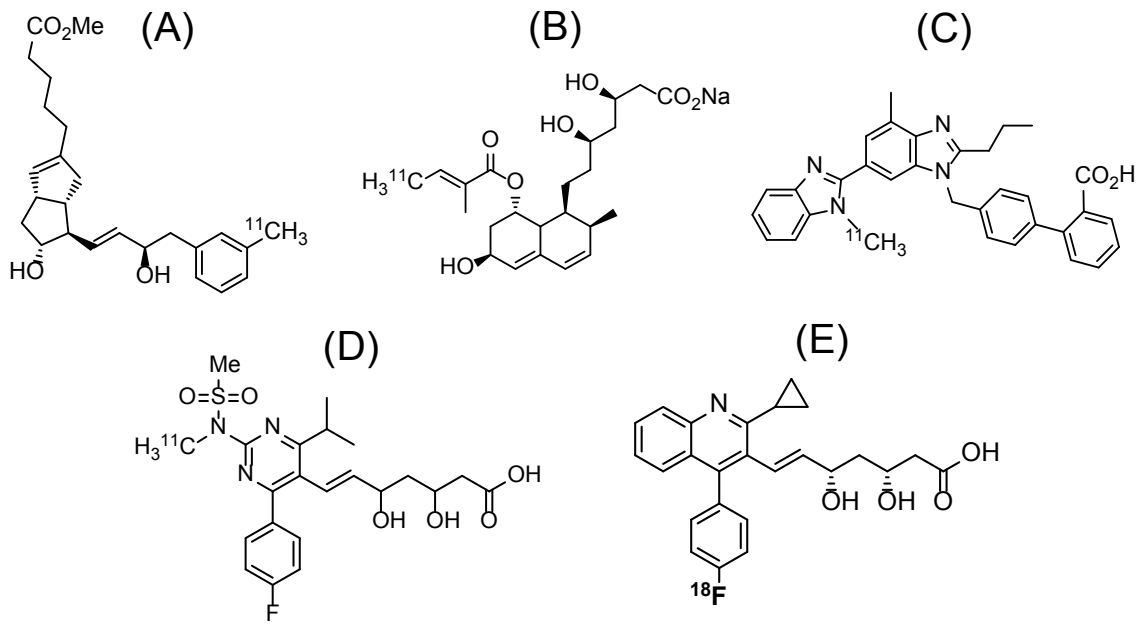2 ‡<0.005) Inset figures show the data points within 5 min

3 **Figure 4.** (A) Integration plots were drawn for the calculation of hepatic uptake of total

4 radioactivity in control and rifampicin-treated rats. The data represent the mean ± SD (n=3).

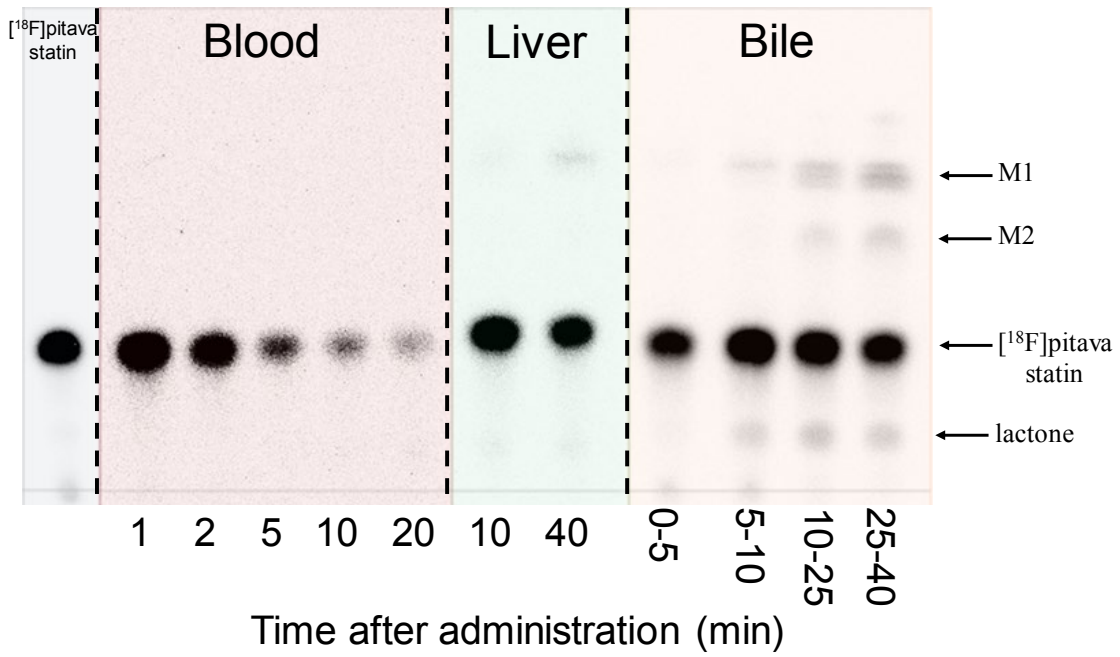5 (B) [^{18}F]pitavastatin's pharmacokinetic parameters after its intravenous administration in rats.

6 The values represent the mean ± SD (n=3; Students t-test, * $p<0.05$)

7

1

2   **Figure 1**
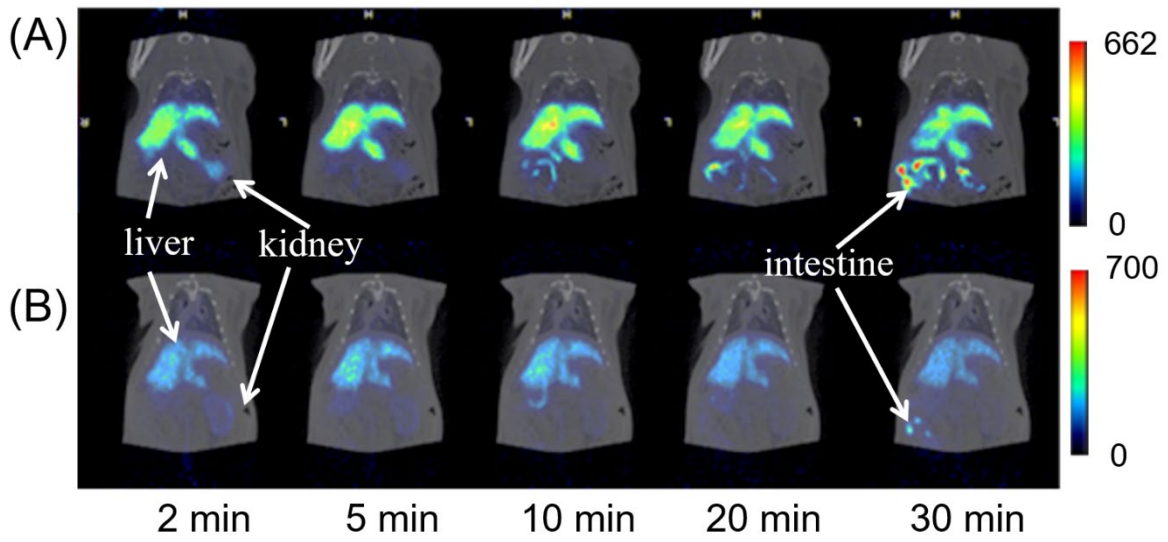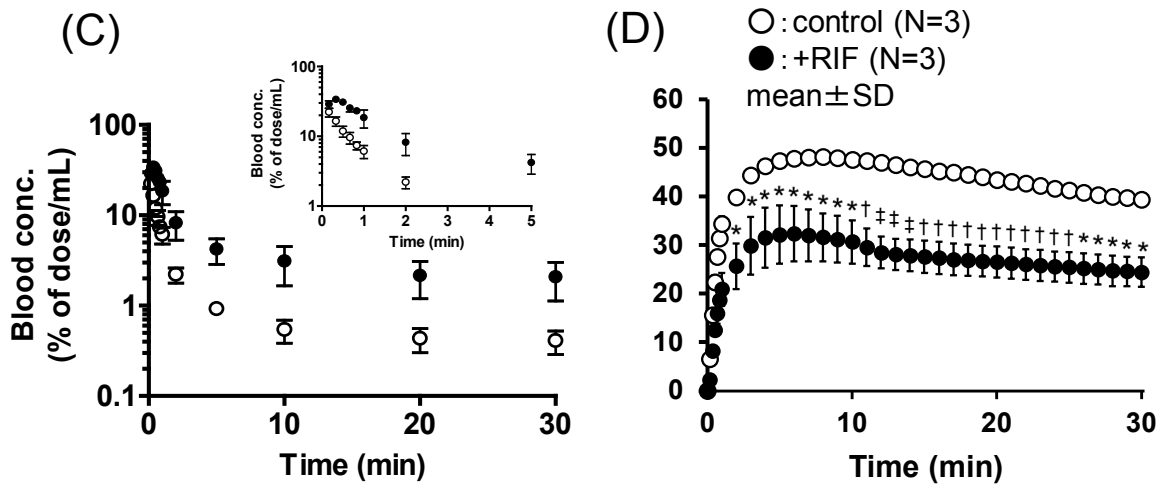
3

Time after administration (min)

4   **Figure 2**

5

1

2

3

(C)

(D)

○ : control (N=3)
● : +RIF (N=3)
mean±SD

4

Figure 3

6

1

(A)
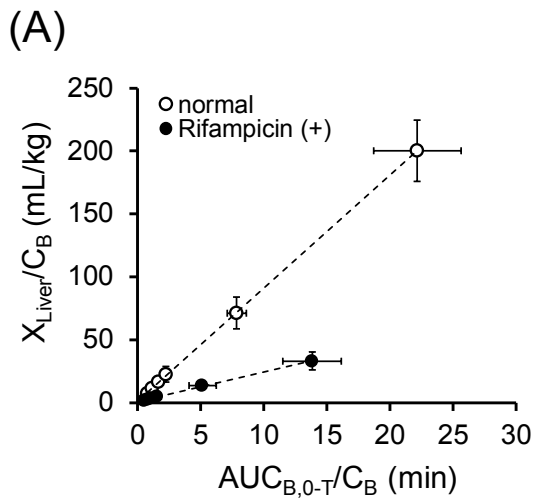
(B)

	normal	Rifampicin (+)
AUCblood,0-30 (%ID·min/mL)	33.1 ± 5.0	111.4 ± 34.9*
CLuptake liver (mL/min/kg)	9.08 ± 1.33	2.33 ± 0.11*

mean±SD (n = 3), * : $p < 0.05$ (*t*-test)

2

3 **Figure 4**

4